CHAPTER V

DIRECT METHYLATION OF BENZENE WITH METHANE OVER Ag/HZSM-5 CATALYST

5.1 Abstract

Methylation of benzene to xylenes using methane as an alkylating agent is a goal of this work. Ag/HZSM-5 catalyst was selected to be studied for its activity of this reaction. Cluster size and oxidation state of Ag species present in Ag/HZSM-5 are proposed to be the important parameters controlling the catalytic activity. Calcination of Ag/HZSM-5 under different environments (e.g., 100% N_2, 5%H_2/N_2, and 100%O_2) led to different Ag species (e.g., Ag^+, Ag_m^0 ($3 \leq m \leq 5$), $Ag_n^{\delta+}$ ($2 \leq n \leq 4$)) in Ag/HZSM-5 catalysts. It was found that only catalyst treated by 5%H_2/N_2 provides $Ag_n^{\delta+}$ ($2 \leq n \leq 4$) and can catalyze the reaction to yield xylenes with some of toluene and C_9+ aromatics. On the other hand, catalysts containing Ag^+ or Ag^+ and Ag_m^0 species are unable to catalyze this reaction. Therefore, $Ag_n^{\delta+}$ species were proposed to be responsible for the methylation reaction into xylenes. However, the stability of $Ag_n^{\delta+}$ under the reaction conditions is very poor, as evidenced by the rapid drops in benzene conversion and product yield. Reduction of $Ag_n^{\delta+}$ into Ag metal particle and reoxidation of $Ag_n^{\delta+}$ into Ag^+ species in Ag/HZSM-5 catalyst during the reaction are possibly the main causes of catalyst deactivation. Moreover, adding H_2 into the feed can prolong catalyst life with enhancing the activity. The effect of methane to benzene feed ratio and space velocity on catalyst activity and stability are also investigated.

Keywords: Methylation, Benzene. Methane, Ag/HZSM-5, UV-Vis DRS, H_2-TPR

5.2 Introduction

Methylation of benzene with methane into higher valuable product (e.g. *p*-xylene) is very attractive due to an increasing price of xylene with an abundance of methane. Due to the thermodynamic limitation, accomplishing this reaction with high *p*-xylene or even toluene yield is quite difficult. Nevertheless, there are some efforts demonstrating the feasibility of this reaction using metal-doped zeolite catalyst. He and co-worker (He et al., 1995) reported the methylation reaction of benzene with methane over Cu/beta and Cu/ZSM-5 catalyst at high temperature and high pressure in a batch rector, the reaction yielded toluene, xylenes, and heavy aromatics as the reaction products. Other works also showed the abilities of Pt/HZSM-5 (Lukyanov et al., 2009) and Ag/HZSM-5 (Baba, 2005; Baba and Sawada, 2002; Baba et al., 2002) catalysts to catalyze this reaction into toluene and xylenes. In addition, the methylation reaction was also tested in the presence of oxygen by using MCM-41 and other zeolites as the catalyst and it was suggested that oxygen is essential to partially oxidize methane into methanol, which subsequently methaylates benzene (Adebajo et al., 2000; Adebajo, 2007; Adebajo et al., 2005; Adebajo et al., 2000). However, CO and CO_2 could simultaneously occur due to oxidation of methane (Adebajo, 2007; Baba and Sawada, 2002).

It is well known that methane has relatively low activity to react with other substances. Therefore, converting methane to more reactive species is suggested in order to perform the reaction of methane. Methane can be activated to the form of carbenium ion (CH_3^+) which should be able to methylate benzene through electrophilic substitution, a most feasible reaction pathway. It has been reported that metal loaded HZSM-5 zeolites are capable of activating methane into highly polarized $CH_3^{\delta+}$ active species (Baba, 2005; Baba et al., 2003; Baba et al., 2007; Baba et al., 2002). Among metal-loaded HZSM-5, Ag/HZSM-5 shows the best activity for methane activation and is used to catalyze the reaction between ethylene and methane into propylene (Baba et al., 2007; Baba and Sawada, 2002). Moreover, Ag loaded Y zeolite is also active for this reaction (Baba et al., 2002). Ag/HZSM-5 was also studied for its activity for the methylation of benzene with methane (Baba, 2005; Baba and Sawada, 2002), the non-oxidative methane coupling reaction (Miao

et al., 2004; Yoshida et al., 2003), the photocatalytic decomposition reaction of N_2O (Matsuoka et al., 2003) and the selective catalytic reduction reaction (SCR) of NO by propane (Shibata et al., 2004; Shibata et al., 2004). The form of Ag in Ag/HZSM-5 and in Ag/Y was further investigated to identify what Ag species is the active species for each reaction. Ag^+ cation was proposed as an active species for the non-oxidative methane coupling reaction (Miao et al., 2004), the photocatalytic decomposition reaction of N_2O (Matsuoka et al., 2003) and the selective reduction of NO to N_2 (Shimizu et al., 2001). On the other hand, silver cationic cluster $(Ag_n^{\delta+})$ was responsible for the methylation of ethylene with methane (Baba et al., 2007) and the selective catalytic reduction reaction (SCR) of NO by propane (Shibata et al., 2004; Shibata et al., 2004). Metallic silver clusters (Ag_m^0) are responsible for the hydrocarbon combustion and N_2O formation in SCR of NO by n-hexane on Ag/Al_2O_3 (Shimizu et al., 2001).

By using an ion-exchange technique, Ag in Ag/HZSM-5 is more likely to be in the Ag^+ cation form. However, this form is rather susceptible to change depending on environmental conditions. Ag^+ cations in zeolite are easily reduced by hydrogen under thermal conditions into metallic Ag^0 and acidic proton (Beyer, 1976; Tsutsumi, 1972; Riekert, 1969; Lins et al., 2004), as shown below:

$$ZO^-Ag^+ + \frac{1}{2}H_2 \rightarrow Ag^0 + ZO\text{-}H \tag{5.1}$$

where ZO^- is the negative framework charge of the zeolite and ZO-H is a Brönsted acid site.

Metallic Ag^0 can further combine with Ag^+ cation to form Ag_n^+ cationic cluster as shown in Eq. (5.2) and Ag_n^+ cationic cluster can also react with hydrogen to form silver hydride (Ag-H) and acidic protons, corresponding to Eq. (5.3) heterolytic cleavage of H_2 or can be further reduced into metallic Ag_m^0 cluster. However, the reduced Ag metal, Ag_n^+ cationic cluster, and silver hydride, which are the products from the reaction (5.1) - (5.3) respectively, can also be reversibly converted into charge-balancing Ag^+ cations by reacting with nearby acidic protons. This reversed

reaction is the so-called "reversible interconversion" (Ausavasukhi et al., 2008; Baba et al., 2002).

$$ZO^-Ag^+ + (n-1)Ag^0 \rightarrow ZO^-Ag_n^+ \tag{5.2}$$

$$ZO^-Ag_n^+ + H_2 \rightarrow Ag_n\text{-}H + ZO\text{-}H \tag{5.3}$$

Due to the existence of only a few works demonstrating the methylation reaction of benzene with methane over-Ag/HZSM-5 catalyst, in the present work, this Ag/HZSM-5 catalyst is selected to be studied for this reaction. The different Ag species in Ag/HZSM-5 were prepared by calcining $AgNO_3$ loaded HZSM-5 under different atmospheres (i.e., N_2, H_2/N_2 and O_2), as reported by Yuvaraj et al. (Yuvaraj, 2003). Linkage between Ag species in Ag/HZSM-5 catalyst and the catalytic activity are discussed. Moreover, the effect of reaction parameters, such as amount of H_2 co-feed, methane to benzene molar ratio, and space velocity, were also studied to assess the catalytic performance as well as the stability of the catalyst.

5.3 Experimental

5.3.1 Catalyst Preparation

The NH_4ZSM-5 (Si/Al: 23) was purchased from Tosoh Corporation. To obtain HZSM-5, NH_4ZSM-5 was calcined at 550 °C for 7 h in a muffle furnace. Subsequently, Ag loaded HZSM-5 was prepared by using a conventional liquid ion-exchange technique (Li, 1997). Silver nitrate ($AgNO_3$) purchased from Merck was used to prepare the Ag precursor solution. Calculated amounts of HZSM-5 and Ag solution were mixed and continuously stirred for 12 h under ambient conditions. After that, Ag/HZSM-5 was separated from the mixture by vacuum filtration and then washed with deionized water until the rinse water had zero conductivity. Washed Ag/HZSM-5 was dried at 120 °C for 12 h in an oven. To create the different Ag species in Ag/HZSM-5, the catalyst was calcined at 350 °C under different environments, which are in $100\%N_2$, $5\%H_2/N_2$, and $100\%O_2$, inside a reactor.

Ag/HZSM-5(N), Ag/HZSM-5(H), Ag/HZSM-5(O) catalysts are designated for the catalysts obtained from calcination under N_2, H_2/N_2, and O_2, respectively.

5.3.2 Catalyst Characterization

Powder X-ray diffraction (XRD); X'Pert Pro MPD PW3040/60 using Cu Kα radiation, was utilized to check the crystallinity of ZSM-5 and the stable phase of Ag. The diffractrogram of the catalyst sample was recorded for 2θ in the range of 5-65° with a scanning speed of 5° min^{-1}. X-ray fluorescence (XRF); AXIOS PW4400, was applied for elemental analysis of catalyst samples. UV-Vis diffuse reflectance spectroscopy (UV-Vis DRS); SHIMADZU UV-2550, was employed for investigating the form of Ag in the Ag/HZSM-5 catalyst with using HZSM-5 as a reference. The spectra were recorded in absorbance mode from the wavelength of 600 nm to 200 nm. Temperature-programmed reduction (TPR); ThermoFinnigan TPDRO 1100 using a TCD detector, was used for determining the reduction temperature of isolated Ag cations as well as that of $Ag_n^{\delta+}$ cationic clusters via the H_2-TPR profile. TPR of the sample was programmed from 50 °C to 750 °C with a ramp rate of 10°C/min under a flow of 4.95% H_2 in N_2 (30 ml/min) and the TCD signal versus sample temperature was recorded. N_2 adsorption-desorption; A Quantachrome Autosorb-1MP instrument, was utilized to measure the surface area and the pore properties of catalyst samples. Surface area was calculated by the BET method, while pore properties were determined by the Non-Local Density Functional Theory (NLDFT) model. Field emission scanning electron microscopy (FE-SEM); A Hitachi S-4800 instrument, was used to investigate the morphology and estimate the particle size of the catalyst samples. Moreover, the elements located on the surface of catalyst samples were also detected by energy dispersive X-ray spectroscopy (EDX), equipped with this FE-SEM.

5.3.3 Catalytic Activity Testing

The reaction between benzene and methane was carried out in a fixed-bed flow reactor, made of quartz (8.4 mm inside diameter and 40 cm length), under non-oxidizing conditions at atmospheric pressure. Catalysts were packed into a quartz tube reactor at the middle of the reactor with bounding at each side (top and

bottom) by quartz wool. A quartz tube was used to support the catalyst bed and also help to reduce reactor volume, thus increasing the product flow. Prior to catalytic measurements, the packed catalyst was heated (10°C/min) to 120°C under N_2 flow (30 ml/min) and held for 30 min in order to remove humidity. Subsequently, it was calcined at 350 °C for 30 min under different atmospheres, and then flushed with N_2. The reactant feed stream was prepared by feeding liquid benzene into a vaporizer operated at 40 °C. Saturated benzene at 40 °C was then carried by N_2 into a mixer, where benzene, methane and nitrogen carrier were mixed prior to feeding to the reactor. The feed stream was first checked by online-GC via a by-pass line before sending to the reactor. The reaction products were analyzed by GC (Agilent 7820A), equipped with an Innowax capillary column and a flame ionization detector (FID), and with a Porapack packed column combined with valve configuration and a thermal conductivity detector (TCD). The first data point was collected at a TOS of 10 min and every 30 min.

5.4 Results and Discussion

5.4.1 Catalyst Characterization

The XRD spectra of HZSM-5 and Ag/HZSM-5 as illustrated in Figure 5.1 clearly show that the structure of ZSM-5 is conserved, but the peaks of either metallic silver ($2\theta = 30°$, $44°$ and $64.5°$) or silver oxide ($2\theta = 33°$ and $38°$) crystals (Wang et al., 2012) cannot be observed, suggesting that silver is possibly present in Ag/HZSM-5 as a charge balancing species (i.e., Ag^+) or a small crystallites without significant long range order. The Ag/HZSM-5 is in the hexagonal shape as portrayed in Figure 5.2 (Left). EDX mapping of Ag confirms the presence of well dispersed Ag on the catalyst surface as shown in Figure 5.2 (Right). The chemical composition, surface area, and pore characteristics of catalyst and HZSM-5 support are summarized in Table 5.1. After adding Ag, Ag/HZSM-5 catalyst still maintains high surface area and pore properties of HZSM-5, indicating that this Ag loading process does not destroy the geometric properties of HZSM-5. Since the pore diameter of this catalyst is 0.614 nm, this catalyst is expected to be more selective toward p-xylenes

than other isomers, because the molecular size of p-xylene is ~0.58 nm and that of m-xylene and o-xylene are ~0.68 nm (Jessica O'Brien-Abraham, 2010).
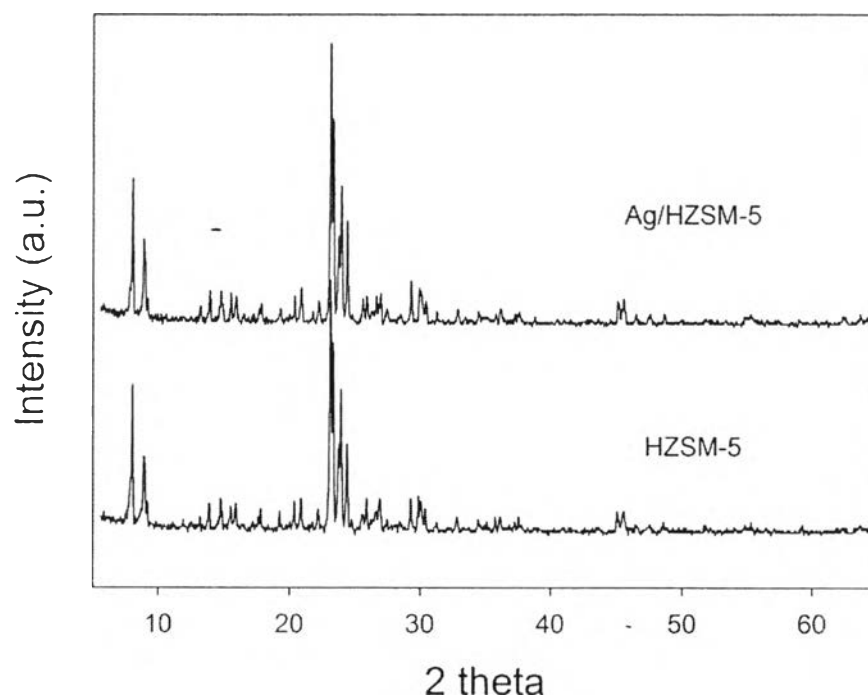

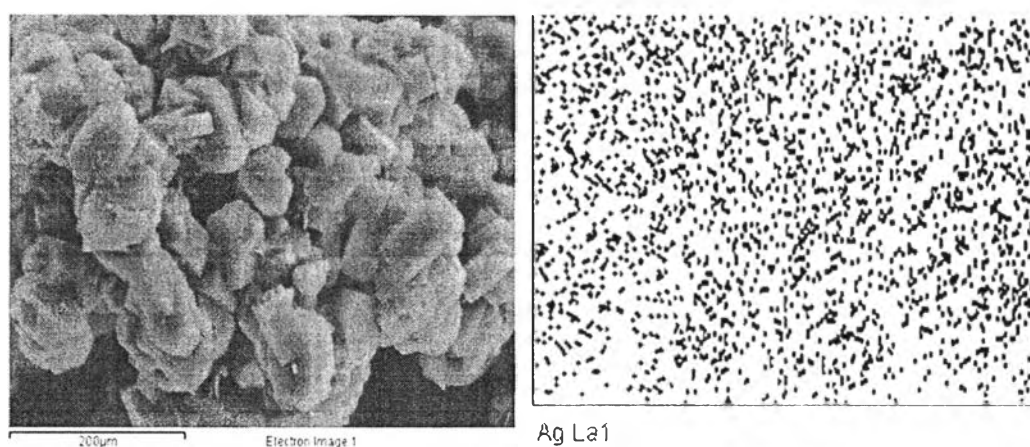**Figure 5.1** Comparative X-ray diffraction patterns of HZSM-5 and Ag/HZSM-5.

Figure 5.2 (Left) FE-SEM image of Ag/HZSM-5, (Right) its corresponding EDX mapping of Ag element.

Table 5.1 Chemical composition. surface area, and pore properties of catalyst samples.

Catalyst	Si/Al[a]	Ag/Al[a]	%Ag (wt%)	BET surface area (m^2/g)	Percentage of micropore[b] (vol%)	Pore diameter[b] (Å)
H-ZSM-5	23	-	-	332.30	_ 100%	6.14
Ag/HZSM-5	23	0.35	2.49	317.30	99%	6.14

[a] Analyzed by using XRF, [b] Determined by NLDFT method

UV-Vis DRS spectra of Ag/HZSM-5 calcined under different atmospheres are illustrated in Figure 5.3. First, Ag/HZSM-5(N) was calcined under a flow of N_2. This catalyst shows two major UV absorption bands. The first band at a wavelength shorter than 250 nm is commonly assigned to the presence of Ag cation in Ag/HZSM-5 (Matsuoka et al., 2003; Miao et al., 2004). This absorption band was described by the electronic excitation of Ag^+ from d^{10} to d^9s^1 under UV irradiation $(Ag^+([Kr]4d^{10}) \xrightarrow{h\nu} Ag^{+*}([Kr]4d^95s^1))$ (Matsuoka, et al., 2005; Shibata et al., 2004; Shibata et al:, 2004; Yoshida et al., 2003). The second peak centered at around 310 nm is assigned to metallic Ag_m cluster ($3 \leq m \leq 5$) (Miao et al., 2004; Shibata et al., 2004; Shibata et al., 2004). The existence of Ag^+ species can also be confirmed by the H_2-TPR result in Figure 5.4 for Ag/HZSM-5(N). The first peak at around 100 °C is attributed to the reduction of isolated Ag cations (Ag^+) (Ausavasukhi et al., 2008; Shibata et al., 2004), while the second peak at around 200 °C is more likely to be Ag cation (Ag^+) inside the pore channel, which is reduced at relatively higher temperature. This is a good evidence for the presence of Ag^+ after calcination. Since Ag can subsequently transform, a large broad peak at high temperature was observed. This peak can be described by Eq. (5.4) (Baba, 2005; Baba et al., 2002; Lins et al., 2004), which is the reduction of Ag_n^+ cationic cluster. Again, a combination between Ag^0 (a product from the first reduction) and a nearby remaining Ag^+, according to Eq. (5.2) (Ausavasukhi et al., 2008; Shibata et al., 2004), leads to the formation of a Ag_n^+ cationic cluster which is reduced at higher

temperature compared to the Ag^+ cation form. Therefore, following calcination under N_2 flow, Ag^+ and Ag_m^0 cluster ($3 \leq m \leq 5$) species are likely to dominate in Ag/HZSM-5(N) catalyst.

$$ZO^-Ag_n^+ + \frac{1}{2}H_2 \rightarrow Ag_n^0 + ZO\text{-}H \tag{5.4}$$

For the sample treated by H_2, Ag/HZSM-5(H) was treated under flow of $5\%H_2$ in N_2 and its UV-Vis DRS spectrum is shown in Figure 5.3. The spectrum illustrates the peaks of Ag^+, metallic Ag_m cluster ($3 \leq m \leq 5$) and, interestingly, $Ag_n^{\delta+}$ cationic cluster ($2 \leq n \leq 4$) which appears at around 260 nm and 285 nm (Shibata et al., 2004; Shibata et al., 2004; Shimizu et al., 2007). Identification of $Ag_n^{\delta+}$ cationic cluster species using UV-Vis DRS approach has been widely studied by many research groups (Miao et al., 2004; Sato et al., 2003; Shibata et al., 2004; Shibata et al., 2004; Shimizu et al., 2007). Sato et al. assigned the bands in the ranges of 238-272 and 275-326 nm to $Ag_n^{\delta+}$ cationic cluster ($2 \leq n \leq 4$) and metallic Ag_m clusters ($3 \leq m \leq 5$), respectively (Sato et al., 2003). Shibata et al. studied the H_2 treatment of Ag/HZSM-5 and proposed the bands at 260 and 285 nm are due to the $Ag_n^{\delta+}$ cationic clusters ($2 \leq n \leq 4$), and assigned the band at 250 and 312 nm to metallic Ag_m clusters ($3 \leq m \leq 5$) (Shibata et al., 2004). Miao et al. proposed the band at 282 nm and 322 nm to the $Ag_n^{\delta+}$ cationic cluster after studying H_2 treatment of Ag/HZSM-5 at 200 °C (Miao et al., 2004). The UV-Vis DRS is in good agreement with the H_2-TPR profile depicted in Figure 5.4 for Ag/HZSM-5(H) catalyst. A small peak left at low temperature indicates that a small fraction of Ag^+ remains unreduced after calcination under H_2/N_2. As most Ag^+ species are reduced and transformed into $Ag_n^{\delta+}$ cationic cluster, the prominent reduction peak of $Ag_n^{\delta+}$ cationic clusters was observed in Ag/HZSM-5(H), as clearly seen by the broad peak centered at around 550 °C. Nevertheless, not only was $Ag_n^{\delta+}$ a resulting Ag species after reduction under H_2/N_2, but also a metallic Ag_m cluster species was identified, as shown by the UV-Vis DRS spectrum.
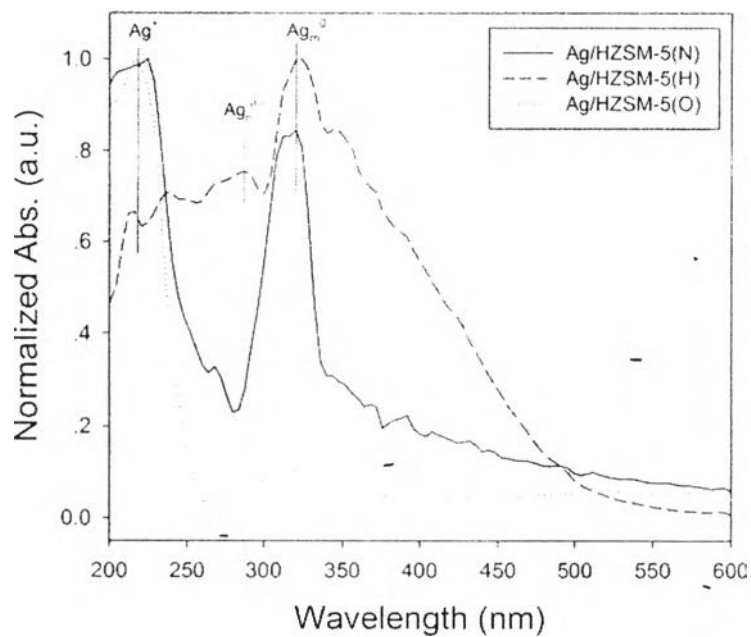
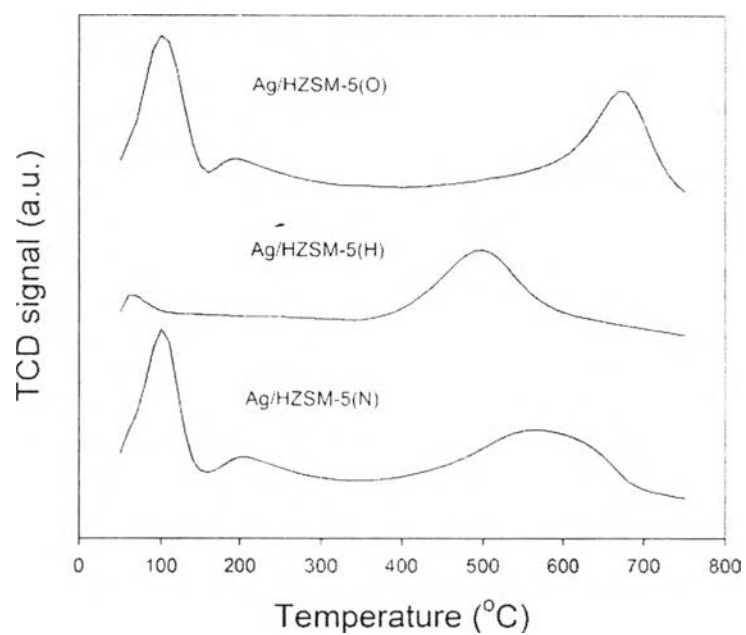**Figure 5.3** Normalized UV-Vis DRS spectra of Ag/HZSM-5 catalysts calcined under different atmospheres.

Figure 5.4 H$_2$-TPR profiles of Ag/HZSM-5 catalysts calcined under different atmospheres.

For the Ag/HZSM-5(O) which was calcined under flow of O_2 at 550 °C, the UV-Vis DRS spectra for Ag/HZSM-5(O) clearly illustrates that Ag/HZSM-5(O) catalyst contains only Ag^+ cation, as it can be observed only a strong absorption band at wavelengths shorter than 250 nm (Figure 5.3). This result is in good agreement with the H_2-TPR result (Figure 5.4) of Ag/HZSM-5(O), in which the reduction of Ag^+ cation was observed. This confirms the existence of Ag^+ cation at the initial state. Therefore, it is most likely that silver in Ag/HZSM-5(O) are all in the form of Ag^+ cation associated with Brönsted sites. Comparing the TPR profiles of all the catalysts in Figure 5.4, it was found that the reduction temperatures of $Ag_n^{\delta+}$ cationic cluster in each catalyst are different. $Ag_n^{\delta+}$ cationic cluster was reduced at 490 °C, 570 °C, and 670 °C in Ag/HZSM-5(H), Ag/HZSM-5(N), and Ag/HZSM-5(O) respectively. This implies differences in the size of $Ag_n^{\delta+}$ cationic cluster in each catalyst. Ag/HZSM-5(H) seems to provide the largest $Ag_n^{\delta+}$ cationic cluster, while Ag/HZSM-5(O) gives the smallest size, and the size of $Ag_n^{\delta+}$ cationic cluster in Ag/HZSM-5(N) is in between these two. Furthermore, the distribution of $Ag_n^{\delta+}$ cationic cluster size in Ag/HZSM-5(H) and Ag/HZSM-5(O) catalysts was narrower than that in Ag/HZSM-5(N), as evidenced by a narrower peak.

5.4.2 Catalytic Activity Testing and Deactivation Investigation

The cationic Ag in Ag/HZSM-5 was expected to be the active species that can catalyze this methylation via first converting methane into polarized methoxy speices ($CH_3^{\delta+}$) (Baba, 2005; Baba et al., 2007; Baba and Sawada, 2002; Baba et al., 2002). Ag species present in Ag/HZSM-5 can be transformed if the treatment or reaction conditions are changed (Yuvaraj, 2003). In this work, Ag/HZSM-5 catalysts containing different Ag species were investigated to find their ability to catalyze the direct methylation reaction. The reaction was performed at 350 °C, methane to benzene molar ratio of 72, and WHSV of 2.80 h^{-1}. The benzene conversion and product selectivity were collected at time on stream of 10 min and the results are tabulated in Table 5.2. It is obvious that only Ag/HZSM-5(H) can catalyze the reaction between benzene and methane into the xylenes. HZSM-5 and Ag/H-ZSM-5(N) can also activate the reaction but they mainly contributed to the formation of heavy aromatic instead of xylenes. Ag/HZSM-5(O) was not able to

catalyze any reactions. The formation of C_9+ aromatic over HZSM-5 might be activated by acidic protons, where the cracking of benzene takes place (Kennedy et al., 1994). As discussed earlier, Ag/HZSM-5(H) is the only catalyst containing $Ag_n^{\delta+}$ cationic cluster and is the only one able to generate xylenes. Therefore, $Ag_n^{\delta+}$ cationic cluster species are believed to be the most active and selective species for the methylaton of benzene to xylenes. In contrast, Ag_m cluster and Ag^+ cation species are not selective for this reaction, especially Ag^+ cation in Ag/HZSM-5(O) that cannot induce any reactions at these conditions. Baba et. al. have proposed the dissociation of methane over Ag_n^+ cationic cluster in zeolite as shown in the reaction below (Baba et al., 2002):

$$ZO^- Ag_n^+ + CH_4 \rightarrow Ag_n\text{-H} + ZO^{\delta-}CH_3^{\delta+} \quad \quad - \quad \quad (5.5)$$

The heterolytic dissociation of CH_4 allows the formation of silver hydride and a highly polarized methoxy group ($CH_3^{\delta+}$). The mechanism was believed to occur by methane being primarily converted into highly polarized methoxy group ($CH_3^{\delta+}$) species over $Ag_n^{\delta+}$ sites, which then react with the benzene to form the methylated products like toluene and xylenes through electrophilic substitution pathway (Baba, 2005). In the case of xylenes formation, besides the methylation reaction route, toluene disproportionation could also be possible, as the Brönsted acid sites can promote this reaction (Bhaskar et al., 1990). Moreover, toluene disproportionation is thermodynamically more favored than toluene methylation for xylenes formation as discussed in Chapter III. Xylenes formed over Ag/HZSM-5(H) occupied around a third of the product distribution (36.2 mol%), with m-xylene as a dominant xylene isomer. This is corresponding to the thermodynamics basis that m-xylene is the most favorable isomer (Perego et al., 2009). Although Ag/HZSM-5(H) can catalyze the reaction to the desired product, the benzene conversion and selectivity were still very low. Furthermore, its stability was poor, as there was no any product observed at TOS longer than 30 min. Therefore, a deactivation study of the catalyst was conducted.

Table 5.2 Benzene conversion and product selectivity[a]

Catalyst	H-ZSM-5	Ag/HZSM-5(N)	Ag/HZSM-5(H)	Ag/HZSM-5(O)
Conversion (mol%)				
Benzene	0.63	0.93	0.18	0
Product distribution (mol%)				
Toluene	0	7.59	32.34	-
p-Xylene	0	0	13.78	-
m-Xylene	0	0	22.44	-
o-Xylene	0	0	0	-
C9Aromatic+	100	92.41	31.43	-
Xylenes fraction (%)				
p-Xylene	-	-	38.04	-
m-Xylene	-	-	61.96	-
o-Xylene	-	-	0	-

[a] reaction temperature: 350 °C, pressure: 1 atm, methane to benzene molar ratio: 72, WHSV: 2.80 h^{-1}, TOS: 10 min.

Figure 5.5 (Top) shows the UV-Vis DRS spectra of fresh- and spent-Ag/HZSM-5(N) catalysts. It is clearly observed that the absorption peak intensity of metallic Ag_m cluster at around 310 nm decreases after the reaction, while the intensities of the absorption band of isolated Ag^-cations (200-250 nm) and of the band of metallic Ag particle (>350 nm) increase. Therefore, it is possible that metallic Ag_m cluster is partially oxidized into Ag^+ cations according to the reversible interconversion reaction described in Eq. (5.1) and, also, agglomerated with nearby Ag_m cluster to form larger Ag particles (Miao et al., 2004; Shibata et al., 2004; Shibata et al., 2004). Figure 5.5 (Middle) depicts the UV-Vis DRS spectra of fresh- and spent-Ag/HZSM-5(H) catalysts. After the reaction, the intensities of bands corresponding to Ag^+ cations (200-250 nm), metallic Ag_m cluster (310 nm), and Ag particle (>350 nm) increase, while, the intensity of $Ag_n^{\delta+}$ cationic cluster ($2 \leq n \leq 4$)

at 260 nm and 285 nm decrease. Therefore, it was discovered that the deactivation of this active catalyst is presumably caused by the transformation of $Ag_n^{\delta+}$ cationic cluster into the less or non-reactive Ag forms (e.g., Ag^+, Ag_m, and Ag particle) (Ausavasukhi et al., 2008; Miao et al., 2004; Shibata et al., 2004; Shibata et al., 2004), thereby causing a dramatic drop of conversion and the product yield. Figure 5.5 (Bottom) illustrated the UV-Vis DRS spectra of fresh- and spent-Ag/HZSM-5(O) catalysts. It is obvious that the catalyst after use for the reaction still maintains only Ag^+ cations (200-250 nm) without any $Ag_n^{\delta+}$ cationic cluster or metallic Ag fomed. Therefore, Ag^+ cation is quite stable under the reaction conditions. Since this catalyst was unable to catalyze the reaction, it can be concluded that Ag^+ cation is an inactive species for the reaction between benzene and methane at such a low temperature of 350 °C. Nonetheless, at higher temperature (>450 °C), Ag/HZSM-5 can at least activate the transformation of methane (Miao et al., 2004).

Ag/HZSM-5(H) is the suitable catalyst for this reaction at such a low temperature (350 °C). Although the benzene conversion is not satisfactory, it is still interesting that this catalyst can promote the reaction between benzene and methane into xylenes. Due to the poor stability of this catalyst as discussed previously, co-feeding with H_2 was proposed and conducted in this work in order to improve the stability and enhance benzene conversion and product yield. The reason of adding H_2 in the feed is because we found that $Ag_n^{\delta+}$ cationic cluster can be oxidized into Ag^+ cation, an inactive species, at the reaction conditions. Therefore, it was expected that the transformation of $Ag_n^{\delta+}$ cationic cluster could be prevented or at least impeded by H_2.
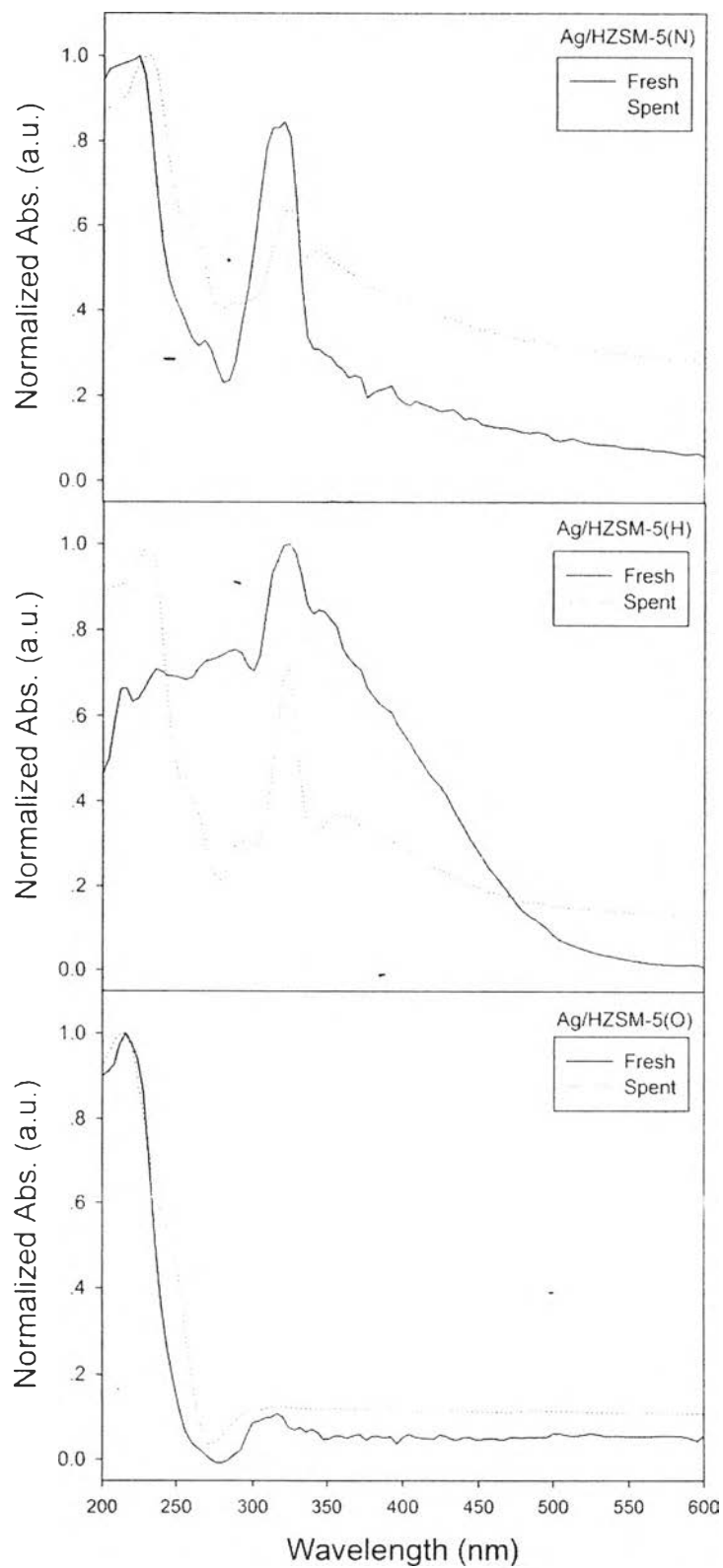
Figure 5.5 UV-Vis DRS spectra of fresh and spent catalysts: (Top) Ag/HZSM-5(N), (Middle) Ag/HZSM-5(H), and (Bottom) Ag/HZSM-5(O).

Table 5.3 Benzene conversion and product selectivity of the reaction with no H_2 co-feed and H_2 co-feed[a]

Catalyst/condition	Ag/HZSM-5(H)	Ag/HZSM-5(H) with H_2 co-feed 3.75 %
Conversion (mol%)		
Benzene	0.18	0.23
Product distribution (mol%)		
Toluene	32.34	32.86
p-Xylene	13.78	10.47
m-Xylene	22.44	13.39
o-Xylene	0	0
C9Aromatic+	31.43	43.28
Xylenes fraction (%)		
p-Xylene	38.04	43.88
m-Xylene	61.96	56.12
o-Xylene	0	0

[a] reaction temperature: 350 °C, pressure: 1 atm, methane to benzene molar ratio: 72, WHSV: 2.80 h^{-1}, TOS: 10 min.

5.4.3 Effect of H_2 Co-feed

Table 5.3 shows the results of benzene conversion and product selectivity of the reaction over Ag/HZSM-5(H) catalyst with/without H_2 in the feed. As expected, H_2 enhanced the activity of the catalyst, namely, with 3.75 % H_2 co-feed, the benzene conversion increased from 0.18 to 0.23 as shown in Table 5.3. This might be because H_2 prolongs the existence of $Ag_n^{\delta+}$ cationic cluster during the reaction with H_2 co-feed, as previously reported in the literature (Shibata et al., 2004). This suggestion is in agreement with the UV-Vis DRS spectra in Figure 5.6. It is clearly observed that for Ag/HZSM-5(H) tested under H_2 co-feed, the peaks of $Ag_n^{\delta+}$ cationic cluster ($2 \leq n \leq 4$) at 260 nm and 285 nm (Shibata et al., 2004; Shibata

et al., 2004) decrease less than that of the Ag/HZSM-5(H) catalyst tested in the absence of H_2. This is a good evidence demonstrating the important role of H_2 in retarding the reversible interconversion of $Ag_n^{\delta+}$ cationic cluster into Ag^+ cations. Notwithstanding, the presence of H_2 during the reaction could also cause the formation of metallic Ag, as its UV-Vis DRS absorption band is evidenced (Shibata et al., 2004). Considering the product selectivity, it is observed that the percentages of toluene and p-xylene selectivity are nearly the same compared with those obtained from the reaction co-fed with H_2. And, m-xylene yield decreased, while heavy aromatic yield increased. It is well known that the acidic proton can promote the formation of heavy aromatic (Kennedy et al., 1994). Hence, an increase in heavier aromatics is likely caused by an increase in acidic proton sites, which might be generated by the H_2 co-feed, and the reaction can be described by Eq. (5.1). Therefore, though H_2 prolongs $Ag_n^{\delta+}$ cationic cluster species for a desired reaction, H_2 also leads to the formation of acidic protons, resulting in more undesirable products.
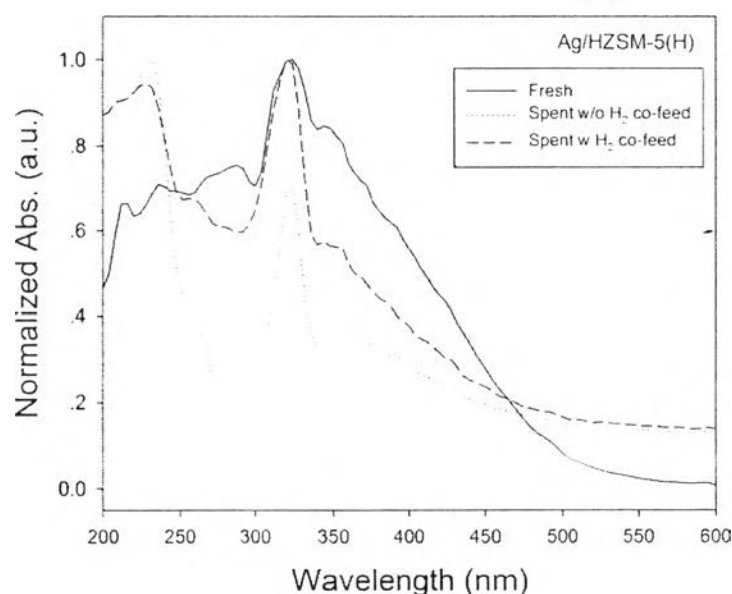

Figure 5.6 Comparative UV-Vis DRS spectra of fresh Ag/HZSM-5(H) and spent Ag/HZSM-5(H) underwent the reaction conditions with/without H_2 co-feed.

Table 5.4 Benzene conversion and product selectivity of the reaction over Ag/HZSM-5(H) catalyst in the presence of H_2 co-feed with varying methane to benzene molar ratio[a]

Methane/Benzene molar ratio	21	72	145
Conversion (mol%)			
Benzene	0.01	0.23	0.30
Product distribution (mol%)			
Toluene	100	32.86	53.90
p-Xylene	0	10.47	22.45
m-Xylene	0	13.39	23.65
o-Xylene	0	0	0
C9Aromatic+	0	43.28	0
Xylenes fraction (%)			
p-Xylene	-	43.88	48.70
m-Xylene	-	56.12	51.30
o-Xylene	-	0	0

[a] reaction temperature: 350 °C, pressure: 1 atm, 3.75% H_2 co-feed, WHSV: 2.80 h^{-1}, TOS: 10 min.

5.4.4 Effect of Methane to Benzene Feed Molar Ratio

Although H_2 co-feed was suggested to prevent the reversible transformation of $Ag_n^{\delta+}$ cationic cluster to Ag^+ cations, however, Ag^+ cation was still present, as its absorption band appeared in the spectrum in Figure 5.6. It is postulated that either benzene or methane can cause the oxidation of $Ag_n^{\delta+}$ cationic cluster. Thus, a study on the influence of methane and benzene contents on the change of Ag species during the reaction was conducted. Also, it was of interest to study the effect of methane to benzene molar ratio on the reaction yield. The varied ratios were 21, 72, and 145. The reaction was tested at 350 °C with 3.75% H_2 co-feed. Table 5.4

shows that benzene conversion increases with increasing methane to benzene molar ratio. At the lowest ratio of 21, the conversion is extremely low and the reaction produce only toluene. An increase in the conversion can be described by *Le Chatelier's* principle. From a product selectivity point of view, it is implied that methylated product like toluene as well as xylenes should be derived from the methylation reaction route as discussed earlier. It is noted that with an abundance of methane the products are only toluene and xylenes. Accordingly, it can be confirmed that heavy aromatics are solely derived from benzene (Kennedy et al., 1994). The catalyst deactivation was investigated using the UV-Vis DRS technique and the resulting spectra are shown in Figure 5.7. As expected, the activity completely dropped with the disappearance of peaks of $Ag_n^{\delta+}$ cationic cluster at around 260 nm and 285 nm (Shibata et al., 2004; Shibata et al., 2004). One should note from Figure 5.7 that the intensity of metallic Ag_m cluster peak increases with increasing methane to benzene molar ratio, while the intensity of the peak for Ag^+ cations becomes lower compared to that of the metallic Ag peak. Therefore, it is more likely that methane can cause the formation of metallic Ag species and benzene possibly causes the formation of Ag^+ cations.
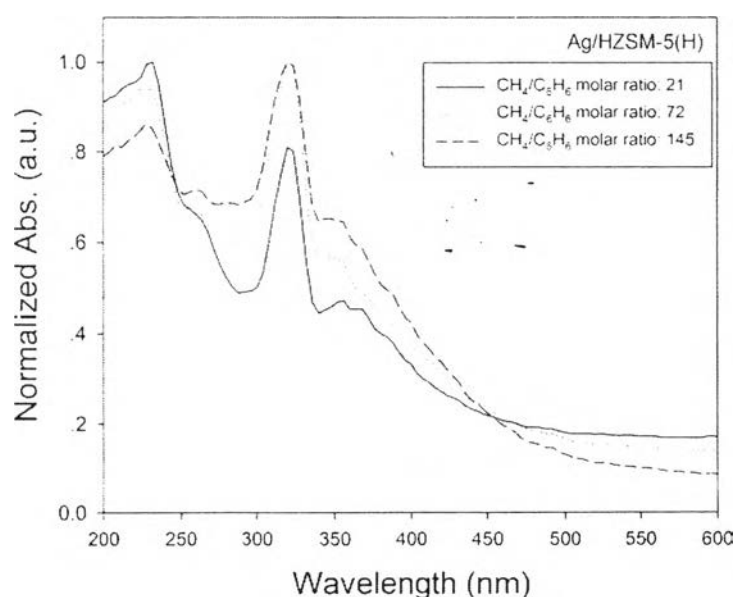

Figure 5.7 Comparative UV-Vis DRS spectra of spent Ag/HZSM-5(H) catalysts run with different methane to benzene molar ratio.

5.4.5 Effect of WHSV

Table 5.5 Benzene conversion and product selectivity of the reaction over Ag/HZSM-5(H) catalyst in the presence of H_2 co-feed with varying space velocity (WHSV)[a]

WHSV (h^{-1})	1.40	2.80	5.60
Conversion (mol%)			
Benzene	2.01	0.23	0.04
Product distribution (mol%)			
Toluene	47.11	32.86	25.33
p-Xylene	5.66	10.47	33.91
m-Xylene	12.03	13.39	40.75
o-Xylene	4.17	0	0
C9Aromatic+	31.03	43.28	0
Xylenes fraction (%)			
p-Xylene	25.89	43.88	45.42
m-Xylene	55.03	56.12	65.58
o-Xylene	19.08	0	0

[a] reaction temperature: 350 °C. pressure: 1 atm, 3.75% H_2 co-feed, methane to benzene molar ratio: 72, TOS: 10 min.

Table 5.5 represents benzene conversion and product selectivity of the reaction over Ag/HZSM-5(H) catalyst in the presence of H_2 co-feed with varying space velocity (WHSV): 1.40, 2.80. and 5.60 h^{-1}. It is clearly that benzene conversion increases with decreasing the WHSV or increasing the contact time between the reactants and catalyst bed. Benzene conversion at WHSV 1.40 h^{-1} was the highest of all. It is reasonable in terms of kinetics that the longer contact time of reactants with catalyst is required for a hardly activated reaction. Moreover, at this low space velocity, o-xylene, one of the xylenes isomers having the lowest thermodynamic

favorability among xylene isomers (Perego et al., 2009), was observed. This implies that the selectivity to the desired product can be controlled by optimizing the space velocity, of which low WHSV toluene is dominant while at high WHSV xylenes dominate.
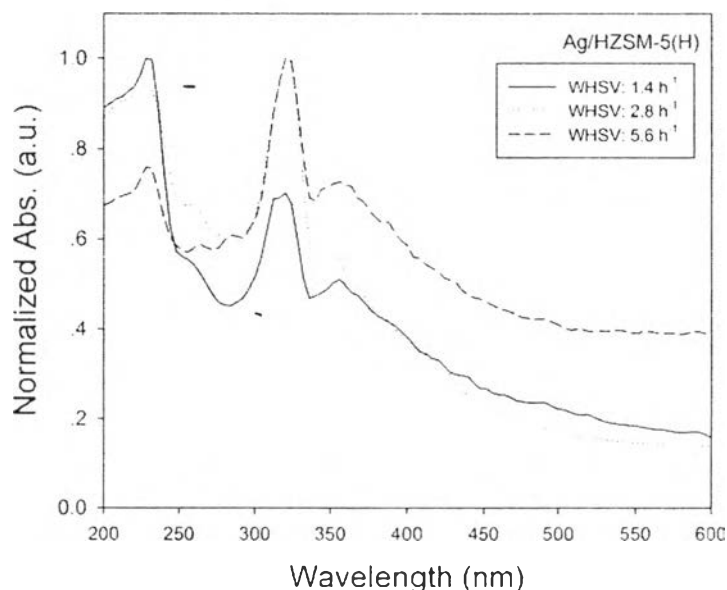

Figure 5.8 Comparative UV-Vis DRS spectra of spent Ag/HZSM-5(H) catalysts run with different WHSV.

Hence, high WHSV seems to be better for xylenes production with diminishing heavy aromatics; however, it is not enough to drive the reaction to satisfactory benzene conversions. Xylenes were possibly generated on the acidic sites of Ag/HZSM-5 via toluene disproportionation (Baba and Sawada, 2002; Perego et al., 2009), which is more thermodynamically favorable than the toluene methylation route. The transformation of $Ag_n^{\delta+}$ cationic clusters into the less reactive species was still the main cause of catalyst deactivation, as observed in Figure 5.8 by the disappearance of the $Ag_n^{\delta+}$ cationic cluster peaks at 260 nm and 285 nm (Shibata et al., 2004; Shibata et al., 2004). Moreover, the peaks of metallic Ag_m cluster (310 nm) and of metallic silver particles (>350 nm) of spent catalyst tested at the highest space velocity (5.60 h^{-1}) show an intensity greater than the peak of Ag^+ cations (200-250 nm). On the other hand, at the lowest space velocity the peak of Ag^+ cations is the

strongest peak. The intensities of the prominent peaks of the spent catalyst for the run with WHSV of 2.8 h^{-1} were in between those of the catalyst run with highest and lowest WHSV. Therefore, it can be concluded that low space velocity (high contact time) preferentially facilitates the formation of Ag^- cations, while high space velocity allows the formation of metallic Ag_m clusters as well as Ag particles.

5.5 Conclusion

This work is the very first to demostrate direct methylation of benzene with methane into xylenes, the desired products. Ag/HZSM-5 containing $Ag_n^{\delta+}$ cation clusters ($2 \leq n \leq 4$) is suggested to be a suitalble catalyst for the reaction. $Ag_n^{\delta+}$ cation cluster in Ag/HZSM-5 catalyst can be obtained by calcination under a $5\%H_2/N_2$ atmosphere. In contrast, calcination under O_2 atmosphere selectively generates only Ag^+ cations and under N_2 atmosphere leads to both Ag^+ cation and metallic Ag species formation. However, these Ag forms can not catalyze the reaction to xylenes. The formation of methylated products, toluene or xylenes, likely proceeded via electrophilic substitution of benzene with highly polarized methyl species, generated from methane on $Ag_n^{\delta+}$ cation cluster. Xylenes are also likely derived from toluene via a toluene disproportionation route on acidic proton sites. The deactivation of the catalyst is likely caused by the transformation of $Ag_n^{\delta+}$ cationic clusters into Ag^+ cations through reversible interconversion and, simultaneously, into metallic Ag through the reduction reaction. Adding H_2 co-feed helps prolong the change of $Ag_n^{\delta+}$ cation cluster during the reaction, resulting in higher benzene conversion. However it can lead to the simultaneous formation of metallic Ag, which causes a dramatic drop in catalytic activity. The higher the methane to benzene molar ratio, the higher the benzene conversion. as expected. Moreover, decreasing the space velocity (WHSV) improves benzene conversion.

5.6 Acknowledgements

5.7 References

Adebajo, M. Long. M.A., and Howe, R.F. (2000) Methane activation over zeolite catalysts: the methylation of benzene. Research on Chemical Intermediates, 26(2), 185-191.

Adebajo, M.O. (2007) Green chemistry perspectives of methane conversion via oxidative methylation of aromatics over zeolite catalysts. Green Chemistry, 9(6), 526-539.

Adebajo, M.O. and Frost, R.L. (2005) Oxidative Benzene Methylation with Methane over MCM-41 and Zeolite Catalysts: Effect of Framework Aluminum, SiO_2/Al_2O_3 Ratio, and Zeolite Pore Structure. Energy & Fuels. 19(3), 783-790.

Adebajo, M.O., Howe, R.F., and Long, M.A. (2000) Methylation of benzene with methanol over zeolite catalysts in a low pressure flow reactor. Catalysis Today, 63(2-4), 471-478.

Ausavasukhi, A., Suwannaran, S., Limtrakul, J., and Sooknoi, T. (2008) Reversible interconversion behavior of Ag species in AgHZSM-5: XRD, ^1H MAS NMR, TPR, TPHE, and catalytic studies. Applied Catalysis A: General. 345(1), 89-96.

Baba, T. (2005) Conversion of Methane over Ag^+-exchanged Zeolite in the Presence of Ethene. Catalysis Surveys from Asia, 9(3), 147-154.

Baba, T. and Abe, Y. (2003) Metal cation–acidic proton bifunctional catalyst for methane activation: conversion of $^{13}CH_4$ in the presence of ethylene over

metal cations-loaded H-ZSM-5. Applied Catalysis A: General, 250(2), 265-270.

Baba, T. and Sawada, H. (2002) Conversion of methane into higher hydrocarbons in the presence of ethylene over H-ZSM-5 loaded with silver cations. Physical Chemistry Chemical Physics, 4(15), 3919-3923.

Baba, T., Iwase, Y., Inazu, K., Masih, D., and Matsumoto, A. (2007) Catalytic properties of silver-exchanged zeolites for propene production by conversion of methane in the presence of ethene. Microporous and Mesoporous Materials, 101(1–2), 142-147.

Baba, T., Sawada, H., Takahashi, T., and Abe, M. (2002) Chemisorption study of hydrogen and methane by ^{1}H MAS NMR and conversion of methane in the presence of ethylene on Ag-Y zeolite. Applied Catalysis A: General, 231(1–2), 55-63.

Beyer, H., Jacobs, P.A., and Uytterhoeven, J.B. (1976) Redox behavior of transition metal ions in zeolites part 2: kinetic study of the reduction and reoxidation of silver-Y Zeolites. Journal of the Chemical Society, Faraday Transactions, 72(1), 674-685.

Bhaskar, G.V. and Do, D.D. (1990) Toluene disproportionation reaction over HZSM-5 zeolites: kinetics and mechanism. Industrial & Engineering Chemistry Research, 29(3), 355-361.

He, S.J.X., Long, M.A., Wilson, M.A., Gorbaty, M.L., and Maa, P.S. (1995) Methylation of benzene by methane-^{13}C over zeolitic catalysts at 400 °C. Energy & Fuels, 9(4), 616-619.

Kennedy, E.M., Lonyi, F., Ballinger, T.H., Rosynek, M.P., and Lunsford, J.H. (1994) Conversion of benzene to substituted aromatic products over zeolite catalysts at elevated pressures. Energy & Fuels, 8(4), 846-850.

Li, Z. and Flytzani-Stephanopoulos, M. (1997) Selective catalytic reduction of nitric oxide by methane over cerium and silver ion-exchanged ZSM-5 zeolites. Applied Catalysis A: General, 165(1-2), 15-34.

Lins, J.O.M.A. and Nascimento, M.A.C. (2004) A density functional study of some silver cluster hydrides. Chemical Physics Letters, 391(1–3), 9-15.

Lukyanov, D.B. and Vazhnova, T. (2009) Selective and stable benzene alkylation with methane into toluene over PtH-MFI bifunctional catalyst. Journal of Molecular Catalysis A: Chemical, 305(1–2), 95-99.

Matsuoka, M., Ju, W.S., Yamashita, H., and Anpo, M. (2003) In situ characterization of the Ag^+ ion-exchanged zeolites and their photocatalytic activity for the decomposition of N_2O into N_2 and O_2 at 298 K. Journal of Photochemistry and Photobiology A: Chemistry, 160(1–2), 43-46.

Matsuoka, M., Lino, K., Chen, H., Anpo, M. (2005) Local structures of Ag (I) clusters prepared within zeolites by ion-exchange method and their photochemical properties. Research on Chemical Intermediates, 31(1-3), 153-165.

Miao, S., Wang, Y., Ma, D., Zhu, Q., Zhou, S., Su, L., Tan, D., and Bao, X. (2004) Effect of Ag^+ cations on nonoxidative activation of methane to C_2-hydrocarbons. The Journal of Physical Chemistry B, 108(46), 17866-17871.

O'Brien-Abraham, J. and Lin, Y.S. (2010) Effect of isomorphous metal substitution in zeolite framework on pervaporation xylene-separation performance of MFI-type zeolite membranes. Industrial and Engineering Chemistry Research, 49, 809-816.

Perego, C. and Pollesel, P. (2009) Advances in aromatics processing using zeolite catalysts. Advances in Nanoporous Materials, 1, 97-146.

Riekert, L. (1969) Redox equilibria in zeolites. Berichte der Bunsengesellschaft für physikalische Chemie, 73(4), 331-338.

Sato, K., Yoshinari, T., Kintaichi, Y., Haneda, M., and Hamada, H. (2003) Remarkable promoting effect of rhodium on the catalytic performance of Ag/Al_2O_3 for the selective reduction of NO with decane. Applied Catalysis B: Environmental, 44(1), 67-78.

Shibata, J., Shimizu, K., Takada, Y., Shichi, A., Yoshida, H., Satokawa, S., Satsuma, A., and Hattori, T. (2004) Structure of active Ag clusters in Ag zeolites for SCR of NO by propane in the presence of hydrogen. Journal of Catalysis, 227(2), 367-374.

Shibata, J., Takada, Y., Shichi, A., Satokawa, S., Satsuma, A., and Hattori, T. (2004) Ag cluster as active species for SCR of NO by propane in the presence of hydrogen over Ag-MFI. Journal of Catalysis, 222(2), 368-376.

Shimizu, K., Shibata, J., Yoshida, H., Satsuma, A., and Hattori, T. (2001) Silver-alumina catalysts for selective reduction of NO by higher hydrocarbons: structure of active sites and reaction mechanism. Applied Catalysis B: Environmental, 30(1-2), 151-162.

Shimizu, K., Sugino, K., Kato, K., Yokota, S., Okumura, K., and Satsuma, A. (2007) Formation and redispersion of silver clusters in Ag-MFI zeolite as investigated by time-resolved QXAFS and UV-Vis. The Journal of Physical Chemistry C, 111(4), 1683-1688.

Tsutsumi, K. and Takahashi, H. (1972) The formation of silver in silver form zeolites. Bulletin of the Chemical Society of Japan, 45, 2332-2337.

Wang, G., Ma, X., Huang, B., Cheng, H., Wang, Z., Zhan, J., Qin, X., Zhang, X., and Dai, Y. (2012) Controlled synthesis of Ag_2O microcrystals with facet-dependent photocatalytic activities. Journal of Materials Chemistry, 22(39), 21189-21194.

Yoshida, H., Hamajima, T., Kato, Y., Shibata, J., Satsuma, A., and Hattori, T. (2003) Active Ag species in MFI zeolite for direct methane conversion in the light and dark. Research on Chemical Intermediates, 29(7-9), 897-910.

Yuvaraj, S., Fan-Yuan, L., Tsong-Huei, C., and Chuin-Tih, Y. (2003) Thermal decomposition of metal nitrates in air and hydrogen environm. The Journal of Physical Chemistry B, 107(4), 1044-1047.